Diel redox cycle of manganese in the surface Arctic Ocean

Yang Xiang[1,1], Phoebe J. Lam[2,2], and Jong-Mi Lee[2,2]

[1]Department of Ocean Sciences, University of California at Santa Cruz
[2]University of California, Santa Cruz

November 30, 2022

Abstract

Knowledge of the chemical speciation of particulate manganese (pMn) is important for understanding the biogeochemical cycling of Mn and other particle-reactive elements. Here, we present the synchrotron-based X-ray spectroscopy-derived average oxidation state (AOS) of pMn in the surface Arctic Ocean collected during the U.S. GEOTRACES Arctic cruise (GN01) in 2015. We show that the pMn AOS is less than 2.4 when sampled during the day and more than ˜3.0 when sampled at night. We hypothesize that an active light-dependent redox cycle between dissolved Mn and particulate Mn(III/IV) exists during the day-night cycle in the surface Arctic Ocean, which occurs on the timescale of hours. The magnitude of observed pMn AOS is likely determined by the net effect of the length of the previous night and integrated light level before the end of pMn sampling.

Diel Redox Cycle of Manganese in the Surface Arctic Ocean

Y. Xiang*, P. J. Lam, J. M. Lee

Department of Ocean Sciences, University of California, Santa Cruz, CA 95064 USA

Corresponding author: Yang Xiang (yaxiang@ucsc.edu)

Key Points:

- Particulate manganese oxidation states are more reduced in the day and more oxidized at night in the surface Arctic Ocean;
- The Mn diel cycle results from the conversion between dissolved Mn and particulate Mn(III/IV) oxides regulated by light;
- The length of night and intensity of light exposure are two main controls on the magnitude of particulate Mn average oxidation states.

Abstract

Knowledge of the chemical speciation of particulate manganese (pMn) is important for understanding the biogeochemical cycling of Mn and other particle-reactive elements. Here, we present the synchrotron-based X-ray spectroscopy-derived average oxidation state (AOS) of pMn in the surface Arctic Ocean collected during the U.S. GEOTRACES Arctic cruise (GN01) in 2015. We show that the pMn AOS is less than 2.4 when sampled during the day and more than ~3.0 when sampled at night. We hypothesize that an active light-dependent redox cycle between dissolved Mn and particulate Mn(III/IV) exists during the day-night cycle in the surface Arctic Ocean, which occurs on the timescale of hours. The magnitude of observed pMn AOS is likely determined by the net effect of the length of the previous night and integrated light level before the end of pMn sampling.

Plain Language Summary

Manganese (Mn) exists in three oxidation states (II, III, and IV) in the ocean. The difference in oxidation states of Mn minerals leads to differences in their capacities to oxidize and sorb other elements, and thereby affects their role in marine redox and nutrient cycling. In this study, we measured the oxidation states of marine particulate Mn in the surface Arctic Ocean. Our results demonstrate a tight coupling between sunlight and particulate Mn oxidation states: more Mn(II) exists in the daytime, whereas more Mn(III/IV) exists during the night. The light-dark cycle is an important driver in the rapid transition between Mn(II) and Mn(III/IV).

Keywords: Manganese; Photoreduction; Oxidation; Arctic Ocean; Synchrotron X-ray fluorescence (XRF); GEOTRACES

1 Introduction

Manganese (Mn) is the 3rd most abundant transition metal in Earth's crust and exists in three oxidation states (II, III, IV) in the ocean. Mn is an essential element to life and used to catalyze the oxidation of water to O_2 in Photosystem II (Yano et al., 2006) by phytoplankton, and to detoxify cells from superoxide radicals via the antioxidant enzyme Mn superoxide dismutase (Peers & Price, 2004). Oxidation from dissolved Mn(II) to particulate Mn(III/IV) oxides is known to proceed through two sequential, one-electron reactions (Luther, 2005). The final oxidation product, Mn(III/IV) oxide, is a strong natural oxidant and is also known as the "scavenger of the sea" (Goldberg, 1954; Tebo et al., 2004). Although Mn is an important micronutrient for phytoplankton growth, dissolved Mn is often characterized by maximum concentrations at the surface ocean (van Hulten et al., 2017) due to photoreduction of Mn(III/IV) oxides (Sunda & Huntsman, 1987, 1994; Sunda et al., 1983) and is thus not typically limiting, except for in the Southern Ocean (Browning et al., 2021; Middag et al., 2013).

Recent GEOTRACES cruises have demonstrated that the Arctic Ocean is enriched in Mn because of riverine, sedimentary and hydrothermal sources (Charette et al., 2020; Colombo et al., 2020; Jensen et al., 2020; Middag et al., 2011; Xiang & Lam, 2020). The Mn concentration in the Western Arctic Ocean is characterized by surface maxima in the Polar Mixed Layer in the dissolved phase and distinct elevations at halocline depths in the particulate phase (Jensen et al., 2020; Xiang & Lam, 2020). Investigations of Mn cycling in the Arctic Ocean have generally focused on processes spanning timescales of several months to years during transport from shelves to central basins. However, a diel cycle in the concentrations of Mn, in both dissolved and particulate phases, has been observed in the coastal Northwest Atlantic Ocean (Oldham et al., 2020; Sunda & Huntsman, 1990).

Here, we use synchrotron-based X-ray absorption spectroscopy (XAS) to examine the chemical speciation of particulate Mn (pMn) and its relationship with light during the U.S. GEOTRACES Arctic cruise (GN01) in 2015. We take advantage of sampling times that spanned a range of light conditions and relatively constant hydrographic parameters throughout the Polar Mixed Layer to reconstruct a pseudo-diel cycle. This study is one of few that focuses on the oxidation state of pMn in the ocean (Hermans et al., 2019; Lee et al., 2021; Oldham et al., 2021), and the first one in the Arctic Ocean. Lee et al. (2021) showed that changes in pMn speciation in the near- vs. far-field 15˚S East Pacific Rise hydrothermal plume were associated with differences in its scavenging affinity for other trace elements and isotopes. Therefore, insights gained in this work help us understand the diel cycling of Mn and potentially also of other pMn-associated elements (e.g., cobalt; Moffett & Ho, 1996) in the surface Arctic Ocean.

2 Materials and Methods

2.1 Marine particle sampling and chemical analysis

Marine particles were sampled using dual-flow McLane Research in-situ pumps (WTS-LV) during the GN01 cruise onboard the U.S. Coast Guard Cutter *Healy* between 9 August and 11 October 2015 (Figure 1). The day-night cycle varied tremendously over the course of the cruise and the length of night ranges from 0 to ~14 hours (Table S1).

Particles (0.8-51 μm) were collected with paired 0.8 μm pore-size polyethersulfone Supor™ filters that were downstream of a 51 μm pore-size polyester pre-filter. Filtered samples were dried in a laminar flow bench at room temperature upon recovery and stored in closed bags

87 in the dark before analysis. Concentrations of pMn were measured by high-resolution inductively
88 coupled mass spectrometry after total digestion (Xiang & Lam, 2020).

89 ### 2.2 Synchrotron X-ray Absorption Spectroscopy (XAS) analysis

90 Surface samples collected at ~20 m depth from 13 stations and one sample within the shelf
91 benthic nepheloid layer, were analyzed by bulk XAS at the Stanford Synchrotron Radiation
92 Lightsource Beamline 11-2. Prior to exposure to the light source, a subsample of the original filter
93 (usually 1/32 of the whole, equivalent to ~12.5 L of pumped seawater) was rolled into multiple
94 layers to maximize the signal from dilute marine particle samples. The speciation of pMn was
95 determined by X-ray Absorption Near Edge Structure (XANES) spectroscopy using a liquid
96 nitrogen cryostat. Averaged spectra were background removed, normalized and deglitched using
97 the SIXPACK software package (Webb, 2005). No obvious shifts of XANES peaks were observed
98 within 10-20 scans in all samples analyzed, indicating no Mn photoreduction had taken place
99 during analysis (Figure S1). To assess variations in the speciation of pMn in the surface Arctic, we
100 calculated the average oxidation state (AOS) of pMn from linear combination fitting of sample
101 XANES spectra in the energy range of 6520-6600 eV using three Mn mineral endmembers to
102 represent three oxidation states (II, III, IV) of Mn (Text S1).

103 ### 2.3 Environmental parameters

104 Environmental parameters that can affect Mn redox cycling such as pH, temperature,
105 oxygen, and light levels (Kim et al., 2012; Sunda & Huntsman, 1994; Toyoda & Tebo, 2016; Von
106 Langen et al., 1997) were measured on the Oceanographic Data Facility (ODF) CTD rosette during
107 the cruise (Landing et al., 2017; Woosley et al., 2017). Photosynthetically available radiation
108 (PAR; wavelength of 400-700 nm) data was collected by a QCP-2300-HP Biospherical PAR

sensor. Since shortwave radiation in the UV-A range (wavelength of 350-380 nm) is thought to contribute most to reduction of Mn(III/IV) oxides (Sunda & Huntsman, 1994), and since PAR data were collected on different casts than particle samples, the solar zenith angle (SZA), defined as the angle between the sun and the vertical plane, is used to estimate the light level in the surface ocean during particle sampling. The SZA is less than 90˚ when the sun is above the horizon ("daylight"), and greater than 90˚ when the sun is below the horizon ("night"). The SZA was calculated with the National Oceanic and Atmospheric Administration Earth Systems Research Laboratory Solar Position Calculator (http://www.esrl.noaa.gov/gmd/grad/solcalc/calcdetails.html) by inputting sampling coordinates and times.

PAR values from the ODF CTD are negatively correlated with their corresponding SZA at 20 decibars during the daytime (SZA<90˚), and they are relatively constant and small at night (SZA>90˚) (Figure 2a). The relationship between PAR and SZA observed during the ODF CTD casts suggests that the magnitude of SZA is a good proxy for visible light levels at 20 m where surface particles were collected, and by extension, possibly for UV-A light as well, given their similar attenuation coefficients (Lee et al., 2013). To account for different weather conditions experienced during the particle sampling at each station, which partly lead to scatter in the relationship between PAR and SZA, we also use underway shortwave radiation (wavelength of ~0.3-3 μm) data measured using a pyranometer above the sea surface at the helicopter deck. Note that underway shortwave radiation data cannot account for variable light attenuation by either ice cover or particles in the water column.

3 Results and Discussion

3.1 Surface pMn speciation

The surface Arctic has median (range) pMn concentrations of 1.0 (0.1-18.7) nmol/L (Table S1). The XANES spectra of surface samples analyzed show a pronounced maximum x-ray absorption peak either at 6561 eV or 6551 eV (Figure 3) which indicates oxidized and reduced pMn, respectively. Oxidized pMn samples (Stations 48, 52, 60) also have a shoulder peak at 6551 eV, reflecting the existence of reduced Mn.

Two distinct x-ray absorption peaks at 6552 and 6557.5 eV occur in the benthic nepheloid layer (BNL) sample (Figure S2). Similar XANES spectra have been observed in estuarine sediments in San Francisco Bay (Carroll et al., 2002) and Baltic Sea sediments (Lenz et al., 2014), potentially suggesting a detrital pool of Mn aluminosilicates. We used the BNL XANES as a likely aluminosilicate reference to fit all surface Arctic samples. Station 6 is the only surface station dominated by the putative Mn aluminosilicates, with the BNL fraction accounting for 68.1% of the XANES signal (Figure S2), suggesting strong sediment resuspension on the Chukchi Shelf. To compare the non-aluminosilicate fraction to other surface samples, the BNL fraction was removed from the bulk XANES spectrum.

The pMn AOS estimated from XANES spectra range from 2.00 to 3.17 (Figure 1 & Table S1). More samples (10 out of 13) were characterized by reduced pMn (AOS<2.9) than oxidized pMn. The most oxidized surface pMn (Station 60; AOS=3.17) was best fit when the Mn(IV) reference (δ-$Mn^{IV}O_2$) was included in the fits (Figure S3). For context, a reasonable expected upper limit for pMn AOS might be the oxidized pMn AOS (3.65) found within the perpetually dark Pacific-derived halocline (Station 14) (Figure S4). Since the measured AOS is the average

oxidation state, it likely includes a mix of Mn(IV) oxides and other forms of pMn with lower oxidation state, such as the pMn(II) found in surface waters (section 3.3).

3.2 Effect of light on pMn speciation

We separate XANES spectra into four groups based on the light level experienced during the 4-hour in-situ sampling and the day-night cycle characterizing that station. The first group experienced full light during sampling, even if a day-night cycle was present at that station (Stations 6, 43, 57, and 66); pMn is generally reduced in this group, characterized by a maximum absorption peak at 6551 eV (Figure 3a). Samples from Stations 43 and 57 also show small peaks at 6561 eV, indicating some presence of oxidized Mn. The second group comprises all surface samples at stations experiencing 24-hour light (Stations 19-38); these spectra exhibit a steep absorption peak at 6551 eV, characteristic of reduced Mn (Figure 3b). A small peak at 6560 eV observed at Station 32 is associated with a high Mn(III) fraction of 19.1% and little Mn(IV) (Table S1). Station 32, characterized by the shortest transport time from the shelf (~6 months) among all surface stations (Kipp et al., 2018), may have received shelf-derived particulate Mn(III/IV) that was transported laterally. The third group of samples were collected in partial darkness and are characterized by reduced Mn (Station 61) or a mixture of reduced and oxidized Mn (Stations 48 and 60) (Figure 3c). The fourth group, comprising only one sample (Station 52), was collected in complete darkness. Similar to the more oxidized samples at Stations 48 and 60, pMn at Station 52 is characterized by a mixture of reduced and oxidized Mn (Figure 3d).

To further describe the relationship between pMn speciation and light, we plot the AOS of pMn against the SZA (Figure 2b). We find that pMn is more oxidized when samples were taken at night (SZA>90˚), whereas it is more reduced when sampled during the day (SZA<90˚). Other

environmental parameters, e.g., temperature, dissolved oxygen, and pH, that are known to influence Mn oxidation (Toyoda & Tebo, 2016; Von Langen et al., 1997) and reduction (Kim et al., 2012; Sunda & Huntsman, 1994) kinetics, do not have clear correlations with pMn AOS in the surface Arctic during our cruise (Figure S5). Therefore, light levels appear to be the first-order control for pMn AOS in the surface Western Arctic.

3.3 Different pMn phases in the surface Arctic

Diel variations in the redox cycling of Mn have been observed in the coastal Northwest Atlantic Ocean (Oldham et al., 2020; Sunda & Huntsman, 1990). Although our data were not conducted at a single location over a 24-hour period, we treat our dataset as a pseudo-diel study and hypothesize that the high pMn AOS in the dark reflects the oxidation of dissolved Mn into Mn(III/IV) oxides at night (Sunda & Huntsman, 1990), and reduced AOS in the light results from the light-dependent reduction of Mn(III/IV) oxides during the day (Sunda & Huntsman, 1988, 1994; Sunda et al., 1983). Photo-enhanced Mn(II) oxidation in the light mediated by reactions with reactive oxygen species has been reported in other environments and laboratory settings (Hansel & Francis, 2006; Learman et al., 2011; Nico et al., 2002). The lower AOS that we observed during the day suggests that light-dependent reduction is more important than photo-enhanced oxidation in the surface Arctic.

Sunda and Huntsman (1990) found that it was the ascorbate reducible fraction of pMn, i.e., Mn(III/IV) oxides, that exhibited a diel pattern, whereas the ascorbate-resistant pMn remained relatively constant throughout the sampling period. We assume the pMn(II) observed in the surface Arctic Ocean is analogous to the ascorbate-resistant fraction noted above. Particulate Mn(II) accounted for a median (range) of 86.2% (23.7-100.0%) of total pMn (Table S1).

196 Ascorbate-resistant pMn could include cellular Mn, adsorbed Mn, and/or Mn(II)-
197 containing minerals. Cellular Mn would presumably be organically-bound, but none of the
198 organically-bound Mn(II) spectra found in the literature (Mn(II)-citrate, Mn(II)-EDTA, Mn
199 superoxide dismutase, or Mn(II)-siderophores) had absorption peaks as low as 6551 eV (Figure
200 S6 & Table S2) (Blamey et al., 2018; Gunter et al., 2006; Harrington et al., 2012; Machado et al.,
201 2019). Mn(II)-containing aluminosilicates are unlikely to be important components of ascorbate-
202 resistant pMn in the surface Arctic, given low concentrations of lithogenic material in the surface
203 (cf., Xiang & Lam, 2020). Of the four Mn(II) adsorption standards we tested, only Mn(II) adsorbed
204 to particulate inorganic carbon (PIC) exhibited an absorption peak close to 6551 eV, although post-
205 edge features were not matched (Figure S6). We previously observed an unknown pMn(II) mineral
206 in a hydrothermal plume (Lee et al., 2021) that contained a similarly low absorption peak at ~6551
207 eV, but like the PIC adsorption standard, also had different post edge features (Figure S7). While
208 we cannot confirm the identity of the observed surface pMn(II), we assume it is in the form of a
209 non-photoactive Mn(II)-containing mineral.

210 We envision a conceptual model with a base level of non-photoactive pMn(II) that remains
211 relatively constant through the day and night. The dissolved Mn pool is in excess of pMn in the
212 surface Arctic Ocean (Jensen et al., 2020). At night, oxidation of ambient dissolved Mn adds
213 pMn(III/IV) to the pMn pool that sinks. The fraction of pMn(III/IV) that remains suspended in the
214 euphotic zone is completely reduced (timescale of hours; Sunda & Huntsman, 1994) and returns
215 to the dissolved Mn pool during daytime. The total pMn concentrations and fractions of
216 Mn(III)+Mn(IV) for oxidized samples collected in the dark from Stations 52 and 60 are 1.1 nM
217 and 64.0%, and 18.7 nM and 76.3%, respectively (Table S1). Assuming all particulate Mn(III/IV)
218 is derived from nightly oxidation of dissolved Mn, we calculate that particulate Mn(III/IV)

concentrations are 0.7 nM at Station 52 and 14.3 nM at Station 60. For simplicity, if we further assume that oxidation starts at dusk and loss of pMn by sinking is small, net Mn oxidation rates can be estimated by dividing the concentration of oxidized Mn by the length of darkness experienced from dusk to the end of sampling at each station (Stations 52 and 60: 6.2 and 2.9 hrs, respectively). Our estimated net Mn oxidation rates at Stations 52 and 60 are 0.11 and 4.9 nM/h, respectively. The much slower apparent oxidation rate at basin Station 52 might be explained by colder temperatures in the basin (~-1.5 °C) compared to 0 °C at Station 60 at the shelf/slope, lower dissolved Mn concentrations (Jensen et al., 2020), and/or by different microbial communities (e.g., Lee et al., 2019) affecting the rates of oxidation. These average rates integrating over 6.2 and 2.9 hours are probably lower than the maximum oxidation rate in the surface Arctic but are generally comparable with other reported microbially mediated Mn oxidation rates of 0.1-50 nM/h in marine environments (Clement et al., 2009; Dick et al., 2009; Sunda & Huntsman, 1990).

3.4 Examination of controls on AOS in the surface Arctic

To examine the controls on the magnitude of pMn AOS, we use the length of night from the SZA data to estimate the extent of oxidation, and calculate the integrated shortwave radiation from dawn to the end of particle sampling for each station to estimate the extent of light-dependent reduction (Table S1). We consider shelf/slope and basin stations separately, since they have very different temperatures (Figure S5), nutrient levels, and light attenuation.

Both the length of night and intensity of light exposure after dawn influence the measured pMn AOS at the time of sampling: a longer period of darkness results in higher AOS at dawn, whereas higher integrated shortwave radiation decreases AOS in the light (Figure 4). We assume that all basin and shelf/slope stations have net Mn oxidation rates the same as Stations 52 (0.11 nM/h) and 60 (4.9 nM/h), respectively (see section 3.3), and estimate the pMn(III/IV) formed at

night by multiplying the length of night at each station by the Mn oxidation rates (Table S1). To estimate the upper bound of AOS at dawn (hereafter the AOS_{dawn}), we use the measured pMn(II) at time of sampling and assume it is constant throughout the day-night cycle and the estimated pMn(III/IV) produced during nighttime oxidation as pMn(IV) to calculate AOS_{dawn} (Figure 4b).

The similar measured AOS at Stations 57 (2.37) and 43 (2.34) belies the different processes at work at these two basin stations: Station 57 had a longer night and thus higher estimated AOS_{dawn}, but it also had higher integrated shortwave radiation by the time of sampling (1.42×10^6 vs. 2.06×10^5 J/m^2), which decreased the AOS greatly (Figure 4a). Station 48 has the highest measured AOS (3.11) as a result of the high estimated AOS_{dawn} (3.65) and the lowest integrated shortwave radiation (1.44×10^5 J/m^2). Fully ice-covered basin Stations 19-38 were sampled under 24-hour light conditions. Despite the expected attenuation in shortwave radiation from ice-cover (e.g., Lund-Hansen et al., 2015), it appears that extended exposure to even attenuated light (>3000 hours) inhibits oxidation and results in low measured AOS (median=2.10) (Figure 2b).

At relatively warm and nutrient-rich shelf stations, higher Mn dark oxidation rates lead to higher estimated AOS (~4) at dawn compared to cold and oligotrophic basin stations (Figure 4b). At Stations 6 and 66, a high magnitude of integrated shortwave radiation (9.21×10^6 and 2.22×10^6 J/m^2, respectively) leads to low measured AOS at the time of sampling (2.03 and 2.11, respectively). It is puzzling, however, to observe low measured AOS (2.11) at Station 61, despite having a high estimated AOS_{dawn} (3.88) and low integrated shortwave radiation (2.35×10^5 J/m^2) (Figure 4a). Factors such as temperature and microbial communities may lead to higher light-dependent Mn reduction rates at the shelf stations compared to basin stations. Alternatively, given the high concentrations of humic substances in the Chukchi Sea (Hioki et al., 2014; Nakayama et al., 2011), it is possible that Mn oxidation at night was inhibited at shelf stations (6, 61, 66) due to

265 strong dissolved Mn(III)-ligand complexes (Oldham et al., 2021). However, the inhibition of Mn
266 oxidation cannot be a universal phenomenon in the Chukchi Sea, since slope Station 60 has a high
267 AOS.

268

269 **4 Conclusions**

270 The observed relationship between the pMn AOS and SZA demonstrates the significance
271 of light in the Mn redox cycling in the Western Arctic Ocean. Such a relationship could also exist
272 in other regions globally, but similar synchrotron-based analyses are more challenging due to much
273 lower pMn concentrations compared to the surface Arctic Ocean.

274 We estimated that the Mn oxidation rate at night in the surface oligotrophic Arctic basins
275 during our cruise is ~0.1 nM/h. Such rates of Mn oxidation take place even within the near-freezing
276 (~-1.5 ˚C) Polar Mixed Layer in late summer. This study serves as the first study to infer in-situ
277 Mn oxidation at such cold temperatures. The oxidation of dissolved Mn(II) in the extended polar
278 winter with no sunlight could serve as a significant seasonal Mn removal mechanism out of the
279 surface layer. Assuming that the Mn oxidation rate remains at 0.1 nM/h in the Arctic winter when
280 it is dark 24 hrs a day, and that riverine and benthic sources of dissolved Mn diminish in winter, it
281 would only take ~50 hours (~2 days) to oxidize the entire reservoir of dissolved Mn in the surface
282 Western Arctic Ocean (~5 nM; Jensen et al., 2020) and then sink out of the Polar Mixed Layer. To
283 our knowledge, no measurements of dissolved or particulate Mn exist in the Arctic winter to test
284 this prediction. Some of these exported Mn oxides during the dark night from the surface could
285 contribute to the ubiquitous layers of sedimentary Mn oxides during interglacial times in the
286 central Arctic Ocean (Löwemark et al., 2014).

287 To date, rapid redox cycles of Mn during the day-night cycle have been observed in the
288 Western Arctic Ocean (this study) and coastal North Atlantic Ocean (Oldham et al., 2020; Sunda
289 & Huntsman, 1990). In contrast, Mn oxidation is absent in the surface Sargasso Sea throughout
290 the day and night, whereas it is present in the dark subsurface (Sunda & Huntsman, 1988). Oldham
291 et al. (2021) did not detect pMn(IV) formation in either sun-lit surface or dark subsurface waters
292 in the Ross Sea. The conditions that govern the diel Mn redox cycle are not clear, but have
293 important implications for availability of Mn and other pMn-associated micronutrients. Future
294 work is needed to investigate the relative importance of light levels, Mn(III)-ligand complexes,
295 microbial communities, and/or reactive oxygen species in controlling Mn redox cycling and its
296 impacts on biogeochemical cycles of different particle-reactive elements.
297

298 **Acknowledgments, Samples, and Data**

299 This work was supported by the Chemical Oceanography program through the National Science
300 Foundation under grant number NSFOCE-1535854 to PJL. This research was carried out at the
301 Stanford Synchrotron Radiation Lightsource, supported by the U.S. Department of Energy, Office
302 of Science, Office of Basic Energy Sciences under Contract No. DE-AC02-76SF00515. We would
303 like to thank all scientists and crew on board the USCGC icebreaker *Healy* during the GN01 Arctic
304 GEOTRACES cruise. We thank co-chief scientist William Landing from Florida State University
305 for providing underway shortwave radiation data, and Susan Becker from the Oceanographic Data
306 Facility (ODF) at Scripps Institution of Oceanography for providing photosynthetically available
307 radiation data. The ODF hydrographic, PAR, and pH data are available on the Biological and
308 Chemical Oceanography Data Management Office (BCO-DMO) (https://www.bco-
309 dmo.org/dataset/700817 and https://www.bco-dmo.org/dataset/646825). The conversion between

voltage and μE/m^2/s in PAR data is based on the calibration conducted before the cruise. Particulate Mn data collected by in-situ pumps in the GN01 cruise are available on the BCO-DMO (https://www.bco-dmo.org/dataset/807340). Many thanks to Ryan C. Davis for the support at the Beamline 11-2, Carl Lamborg and Colleen Hansel for insights in the discussion, Benjamin Twining for providing Mn quota data for discussion, Colleen Hansel for providing XANES reference spectra including δ-MnO_2 and feitknechtite, Jena E. Johnson for Mn silicates reference spectra, Peter Kopittke for Mn citrate and oxalate reference spectra, and Hudson Carvalho for Mn-EDTA reference spectra. Thanks to two anonymous reviewers whose comments helped to improve this manuscript.

References

Blamey, F. P. C., McKenna, B. A., Li, C., Cheng, M., Tang, C., Jiang, H., et al. (2018). Manganese distribution and speciation help to explain the effects of silicate and phosphate on manganese toxicity in four crop species. *New Phytologist*, *217*(3), 1146-1160. https://doi.org/10.1111/nph.14878

Browning, T. J., Achterberg, E. P., Engel, A., & Mawji, E. (2021). Manganese co-limitation of phytoplankton growth and major nutrient drawdown in the Southern Ocean. *Nature Communications*, *12*(1), 884. https://doi.org/10.1038/s41467-021-21122-6

Carroll, S., O'Day, P. A., Esser, B., & Randall, S. (2002). Speciation and fate of trace metals in estuarine sediments under reduced and oxidized conditions, Seaplane Lagoon, Alameda Naval Air Station (USA). *Geochemical Transactions*, *3*(10), 81-101. https://doi.org/10.1039/B205002A

Charette, M. A., Kipp, L. E., Jensen, L. T., Dabrowski, J. S., Whitmore, L. M., Fitzsimmons, J. N., et al. (2020). The Transpolar Drift as a source of riverine and shelf-derived trace elements to

the central Arctic Ocean. *Journal of Geophysical Research: Oceans*, *125*(5). https://doi.org/10.1029/2019jc015920

Clement, B. G., Luther, G. W., & Tebo, B. M. (2009). Rapid, oxygen-dependent microbial Mn(II) oxidation kinetics at sub-micromolar oxygen concentrations in the Black Sea suboxic zone. *Geochimica et Cosmochimica Acta*, *73*(7), 1878-1889. https://doi.org/10.1016/j.gca.2008.12.023

Colombo, M., Jackson, S. L., Cullen, J. T., & Orians, K. J. (2020). Dissolved iron and manganese in the Canadian Arctic Ocean: On the biogeochemical processes controlling their distributions. *Geochimica et Cosmochimica Acta*, *277*, 150-174. https://doi.org/10.1016/j.gca.2020.03.012

Dick, G. J., Clement, B. G., Webb, S. M., Fodrie, F. J., Bargar, J. R., & Tebo, B. M. (2009). Enzymatic microbial Mn(II) oxidation and Mn biooxide production in the Guaymas Basin deep-sea hydrothermal plume. *Geochimica et Cosmochimica Acta*, *73*(21), 6517-6530. https://doi.org/10.1016/j.gca.2009.07.039

Goldberg, E. D. (1954). Marine Geochemistry 1. Chemical Scavengers of the Sea. *The Journal of Geology*, *62*(3), 249-265

Gunter, K. K., Aschner, M., Miller, L. M., Eliseev, R., Salter, J., Anderson, K., & Gunter, T. E. (2006). Determining the oxidation states of manganese in NT2 cells and cultured astrocytes. *Neurobiology of Aging*, *27*(12), 1816-1826. https://doi.org/10.1016/j.neurobiolaging.2005.10.003

Hansel, C. M., & Francis, C. A. (2006). Coupled photochemical and enzymatic Mn(II) oxidation pathways of a planktonic *Roseobacter*-like bacterium. *Applied and Environmental Microbiology*, *72*(5), 3543. https://doi.org/10.1128/AEM.72.5.3543-3549.2006

356 Harrington, J. M., Parker, D. L., Bargar, J. R., Jarzecki, A. A., Tebo, B. M., Sposito, G., &
357 Duckworth, O. W. (2012). Structural dependence of Mn complexation by siderophores: Donor
358 group dependence on complex stability and reactivity. *Geochimica et Cosmochimica Acta*, *88*,
359 106-119. https://doi.org/10.1016/j.gca.2012.04.006
360 Hermans, M., Lenstra, W. K., van Helmond, N. A. G. M., Behrends, T., Egger, M., Séguret, M. J.
361 M., et al. (2019). Impact of natural re-oxygenation on the sediment dynamics of manganese,
362 iron and phosphorus in a euxinic Baltic Sea basin. *Geochimica et Cosmochimica Acta*, *246*,
363 174-196. https://doi.org/10.1016/j.gca.2018.11.033
364 Hioki, N., Kuma, K., Morita, Y., Sasayama, R., Ooki, A., Kondo, Y., et al. (2014). Laterally
365 spreading iron, humic-like dissolved organic matter and nutrients in cold, dense subsurface
366 water of the Arctic Ocean. *Scientific Reports*, *4*, 6775. https://doi.org/10.1038/srep06775
367 Jensen, L. T., Morton, P. L., Twining, B. S., Heller, M. I., Hatta, M., Measures, C. I., et al. (2020).
368 A comparison of marine Fe and Mn cycling: U.S. GEOTRACES GN01 Western Arctic case
369 study. *Geochimica et Cosmochimica Acta*, *288*, 138-160.
370 https://doi.org/10.1016/j.gca.2020.08.006
371 Kim, K., Yoon, H. I., & Choi, W. (2012). Enhanced dissolution of manganese oxide in ice
372 compared to aqueous phase under illuminated and dark conditions. *Environmental Science &*
373 *Technology*, *46*(24), 13160-13166. https://doi.org/10.1021/es302003z
374 Kipp, L. E., Charette, M. A., Moore, W. S., Henderson, P. B., & Rigor, I. G. (2018). Increased
375 fluxes of shelf-derived materials to the central Arctic Ocean. *Science advances*, *4*(1),
376 eaao1302. https://doi.org/10.1126/sciadv.aao1302
377 Landing, W. M., Cutter, G., & Kadko, D. C. (2017). CTD-ODF profiles from GEOTRACES-
378 Arctic Section cruise HLY1502, August to October 2015 (U.S. GEOTRACES Arctic project).

Biological and Chemical Oceanography Data Management Office (BCO-DMO), *Dataset version 2017-05-22*. Retrieved from http://lod.bco-dmo.org/id/dataset/700817

Learman, D. R., Wankel, S. D., Webb, S. M., Martinez, N., Madden, A. S., & Hansel, C. M. (2011). Coupled biotic–abiotic Mn(II) oxidation pathway mediates the formation and structural evolution of biogenic Mn oxides. *Geochimica et Cosmochimica Acta*, *75*(20), 6048-6063. https://doi.org/10.1016/j.gca.2011.07.026

Lee, J., Kang, S. H., Yang, E. J., Macdonald, A. M., Joo, H. M., Park, J., et al. (2019). Latitudinal distributions and controls of bacterial community composition during the summer of 2017 in Western Arctic Surface waters (from the Bering Strait to the Chukchi Borderland). *Scientific Reports*, *9*(1), 16822. https://doi.org/10.1038/s41598-019-53427-4

Lee, J. M., Lam, P. J., Vivancos, S. M., Pavia, F. J., Anderson, R. F., Lu, Y., et al. (2021). Changing chemistry of particulate manganese in the near- and far-field hydrothermal plumes from 15°S East Pacific Rise and its influence on metal scavenging. *Geochimica et Cosmochimica Acta*, *300*, 95-118. https://doi.org/10.1016/j.gca.2021.02.020

Lee, Z., Hu, C., Shang, S., Du, K., Lewis, M., Arnone, R., & Brewin, R. (2013). Penetration of UV-visible solar radiation in the global oceans: Insights from ocean color remote sensing. *Journal of Geophysical Research: Oceans*, *118*(9), 4241-4255. https://doi.org/10.1002/jgrc.20308

Lenz, C., Behrends, T., Jilbert, T., Silveira, M., & Slomp, C. P. (2014). Redox-dependent changes in manganese speciation in Baltic Sea sediments from the Holocene Thermal Maximum: An EXAFS, XANES and LA-ICP-MS study. *Chemical Geology*, *370*, 49-57. https://doi.org/10.1016/j.chemgeo.2014.01.013

Löwemark, L., März, C., O'Regan, M., & Gyllencreutz, R. (2014). Arctic Ocean Mn-stratigraphy: genesis, synthesis and inter-basin correlation. *Quaternary Science Reviews*, *92*, 97-111. https://doi.org/10.1016/j.quascirev.2013.11.018

Lund-Hansen, L. C., Markager, S., Hancke, K., Stratmann, T., Rysgaard, S., Ramløv, H., & Sorrell, B. K. (2015). Effects of sea-ice light attenuation and CDOM absorption in the water below the Eurasian sector of central Arctic Ocean (>88°N). *Polar Research*, *34*(0). https://doi.org/10.3402/polar.v34.23978

Luther, G. W. (2005). Manganese(II) oxidation and Mn(IV) reduction in the environment—two one-electron transfer steps versus a single two-electron step. *Geomicrobiology Journal*, *22*(3-4), 195-203. https://doi.org/10.1080/01490450590946022

Machado, B. A., Gomes, M. H. F., Marques, J. P. R., Otto, R., & de Carvalho, H. W. P. (2019). X-ray spectroscopy fostering the understanding of foliar uptake and transport of Mn by soybean (*Glycine max* L. Merril): Kinetics, chemical speciation, and effects of glyphosate. *Journal of Agricultural and Food Chemistry*, *67*(47), 13010-13020. https://doi.org/10.1021/acs.jafc.9b05630

Middag, R., de Baar, H. J. W., Klunder, M. B., & Laan, P. (2013). Fluxes of dissolved aluminum and manganese to the Weddell Sea and indications for manganese co-limitation. *Limnology and Oceanography*, *58*(1), 287-300. https://doi.org/10.4319/lo.2013.58.1.0287

Middag, R., de Baar, H. J. W., Laan, P., & Klunder, M. B. (2011). Fluvial and hydrothermal input of manganese into the Arctic Ocean. *Geochimica et Cosmochimica Acta*, *75*(9), 2393-2408. https://doi.org/10.1016/j.gca.2011.02.011

Moffett, J. W., & Ho, J. (1996). Oxidation of cobalt and manganese in seawater via a common microbially catalyzed pathway. *Geochimica et Cosmochimica Acta*, *60*(18), 3415-3424. https://doi.org/10.1016/0016-7037(96)00176-7

Nakayama, Y., Fujita, S., Kuma, K., & Shimada, K. (2011). Iron and humic-type fluorescent dissolved organic matter in the Chukchi Sea and Canada Basin of the western Arctic Ocean. *Journal of Geophysical Research: Oceans*, *116*(C7). https://doi.org/10.1029/2010jc006779

Newville, M. (2001). IFEFFIT: Interactive XAFS analysis and FEFF fitting. *Journal of Synchrotron Radiation*, *8*(2), 322-324. https://doi.org/10.1107/S0909049500016964

Nico, P. S., Anastasio, C., & Zasoski, R. J. (2002). Rapid photo-oxidation of Mn(II) mediated by humic substances. *Geochimica et Cosmochimica Acta*, *66*(23), 4047-4056. https://doi.org/10.1016/S0016-7037(02)01001-3

Oldham, V. E., Chmiel, R., Hansel, C. M., DiTullio, G. R., Rao, D., & Saito, M. A. (2021). Inhibited manganese oxide formation hinders cobalt scavenging in the Ross Sea. *Global Biogeochemical Cycles*, *n/a*(n/a), e2020GB006706. https://doi.org/10.1029/2020GB006706

Oldham, V. E., Lamborg, C. H., & Hansel, C. M. (2020). The spatial and temporal variability of Mn speciation in the coastal Northwest Atlantic Ocean. *Journal of Geophysical Research: Oceans*, *125*(1), e2019JC015167. https://doi.org/10.1029/2019JC015167

Peers, G., & Price, N. M. (2004). A role for manganese in superoxide dismutases and growth of iron-deficient diatoms. *Limnology and Oceanography*, *49*(5), 1774-1783. https://doi.org/10.4319/lo.2004.49.5.1774

Sunda, W. G., & Huntsman, S. A. (1987). Microbial oxidation of manganese in a North Carolina estuary1. *Limnology and Oceanography*, *32*(3), 552-564. https://doi.org/10.4319/lo.1987.32.3.0552

Sunda, W. G., & Huntsman, S. A. (1988). Effect of sunlight on redox cycles of manganese in the southwestern Sargasso Sea. *Deep Sea Research Part A. Oceanographic Research Papers*, *35*(8), 1297-1317. https://doi.org/10.1016/0198-0149(88)90084-2

Sunda, W. G., & Huntsman, S. A. (1990). Diel cycles in microbial manganese oxidation and manganese redox speciation in coastal waters of the Bahama Islands. *Limnology and Oceanography*, *35*(2), 325-338. https://doi.org/10.4319/lo.1990.35.2.0325

Sunda, W. G., & Huntsman, S. A. (1994). Photoreduction of manganese oxides in seawater *Marine Chemistry*, *46*, 133-152. https://doi.org/10.1016/0304-4203(94)90051-5

Sunda, W. G., Huntsman, S. A., & Harvey, G. R. (1983). Photoreduction of manganese oxides in seawater and its geochemical and biological implications. *Nature*, *301*(5897), 234. https://doi.org/10.1038/301234a0

Tebo, B. M., Bargar, J. R., Clement, B. G., Dick, G. J., Murray, K. J., Parker, D., et al. (2004). Biogenic manganese oxides: Properties and mechanisms of formation. *Annual Review of Earth and Planetary Sciences*, *32*(1), 287-328. https://doi.org/10.1146/annurev.earth.32.101802.120213

Toyoda, K., & Tebo, B. M. (2016). Kinetics of Mn(II) oxidation by spores of the marine Bacillus sp. SG-1. *Geochimica et Cosmochimica Acta*, *189*, 58-69. https://doi.org/10.1016/j.gca.2016.05.036

van Hulten, M., Middag, R., Dutay, J. C., de Baar, H., Roy-Barman, M., Gehlen, M., et al. (2017). Manganese in the west Atlantic Ocean in the context of the first global ocean circulation model of manganese. *Biogeosciences*, *14*(5), 1123-1152. https://doi.org/10.5194/bg-14-1123-2017

Von Langen, P. J., Johnson, K. S., Coale, K. H., & Elrod, V. A. (1997). Oxidation kinetics of manganese (II) in seawater at nanomolar concentrations. *Geochimica et Cosmochimica Acta*, *61*(23), 4945-4954. https://doi.org/10.1016/S0016-7037(97)00355-4

Webb, S. M. (2005). SIXPack a graphical user interface for XAS analysis using IFEFFIT. *Physica Scripta*, 1011. https://doi.org/10.1238/physica.topical.115a01011

Woosley, R. J., Millero, F. J., & Takahashi, T. (2017). Internal consistency of the inorganic carbon system in the Arctic Ocean. *Limnology and Oceanography: Methods*, *15*(10), 887-896. https://doi.org/10.1002/lom3.10208

Xiang, Y., & Lam, P. J. (2020). Size-fractionated compositions of marine suspended particles in the Western Arctic Ocean: Lateral and vertical sources. *Journal of Geophysical Research: Oceans*, *125*(8), e2020JC016144. https://doi.org/10.1029/2020JC016144

Yano, J., Kern, J., Sauer, K., Latimer, M. J., Pushkar, Y., Biesiadka, J., et al. (2006). Where water is oxidized to dioxygen: Structure of the photosynthetic Mn4Ca cluster. *Science*, *314*(5800), 821-825. https://doi.org/10.1126/science.1128186

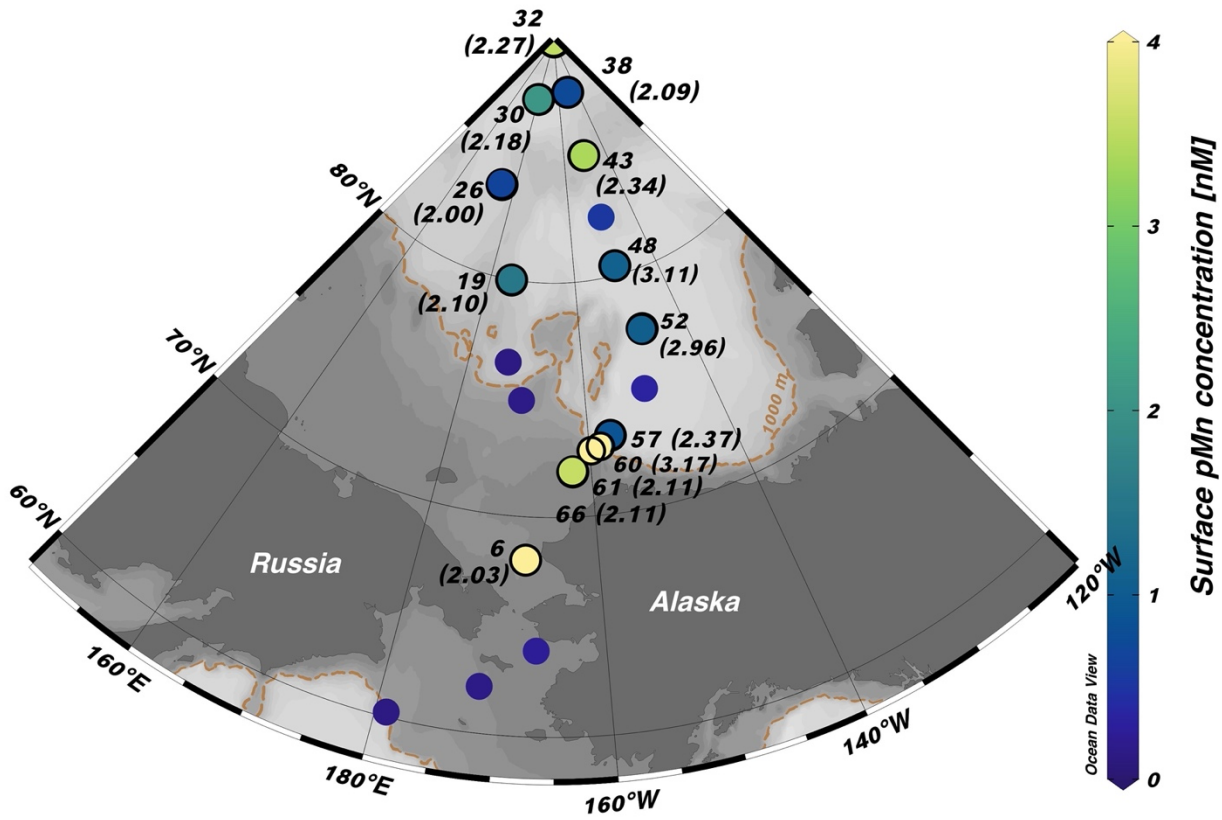

488

489 **Figure 1**. Sampling locations of the GN01 cruise (cruise track: clockwise). Colors show the
490 surface particulate Mn (pMn) concentrations (unit: nmol/L). Average oxidation states (AOS) of
491 pMn analyzed by XANES are labeled next to station numbers within parenthesis.

492

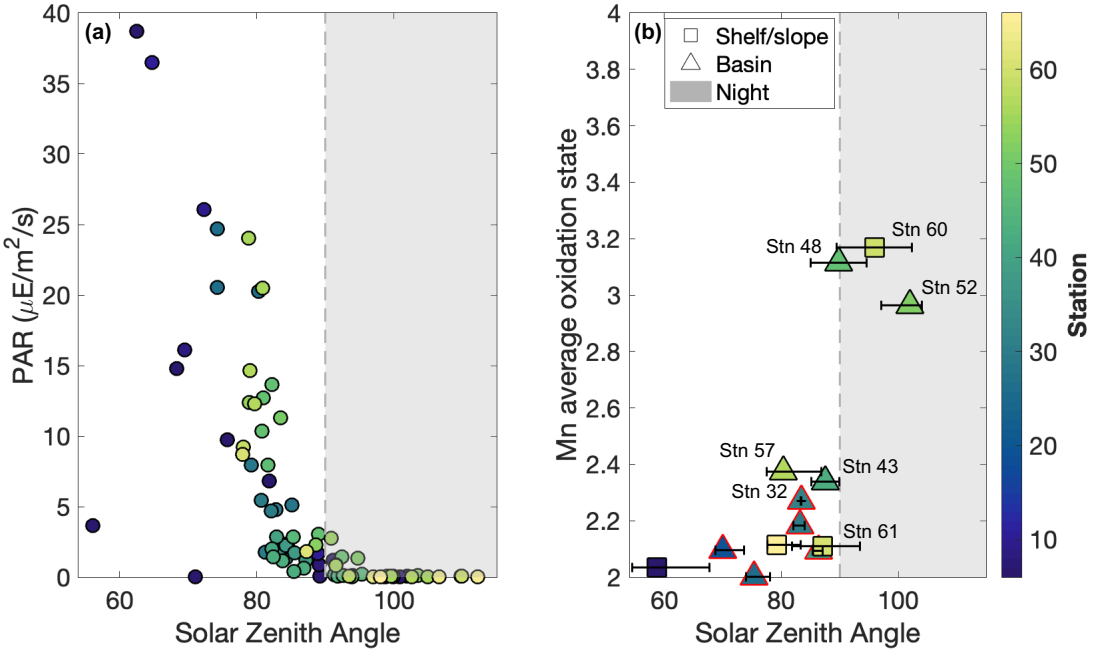

493

494 **Figure 2**. The relationships between SZA and PAR measured in the ODF CTD casts at pressure=
495 20 decibars (a), and between SZA and Mn AOS measured on particles collected in the pump casts
496 at ~20 m (b). The symbols in (b) are the SZA at mid-cast and error bars demonstrate the minimum
497 and maximum SZA during particle sampling. Samples collected under 24-h light conditions are
498 outlined in red.

499

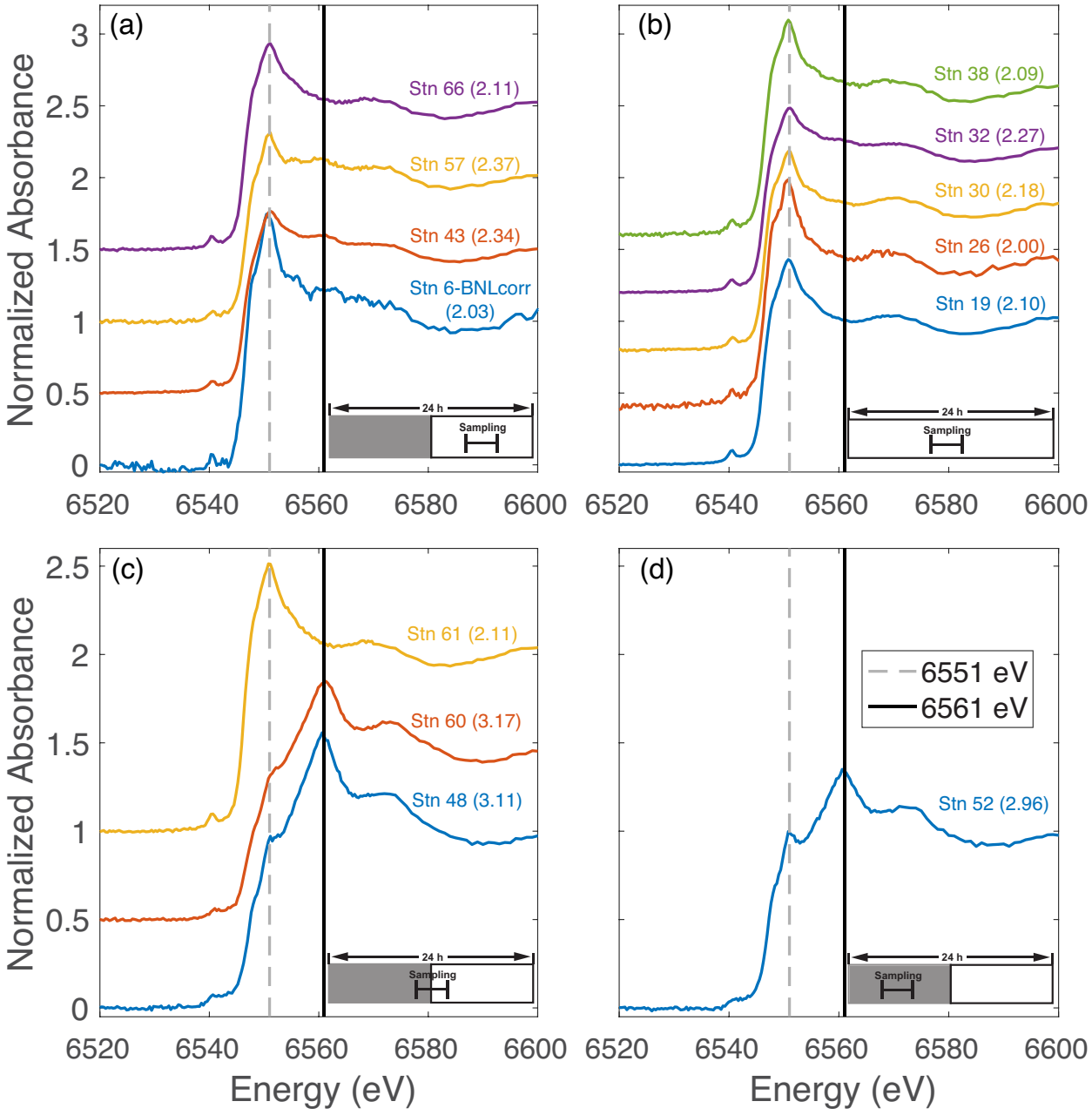

Figure 3. Mn K-edge bulk XANES spectra of surface pMn analyzed, grouped by different light levels experienced during the sampling and/or on a daily basis. The selection criteria for four groups are displayed as a cartoon in the bottom right corner of each subplot, illustrating whether there was a day-night cycle at that station during sampling (white-shaded rectangle) and the light level during sampling (horizontal bar). (a): sampling entirely in the light but experiencing a day-

night cycle; (b): sampling entirely in the light and experiencing 24-h light; (c): sampling partially in the light; (d): sampling entirely in the dark but experiencing a day-night cycle. The pMn AOS for each spectrum is labeled within parenthesis.

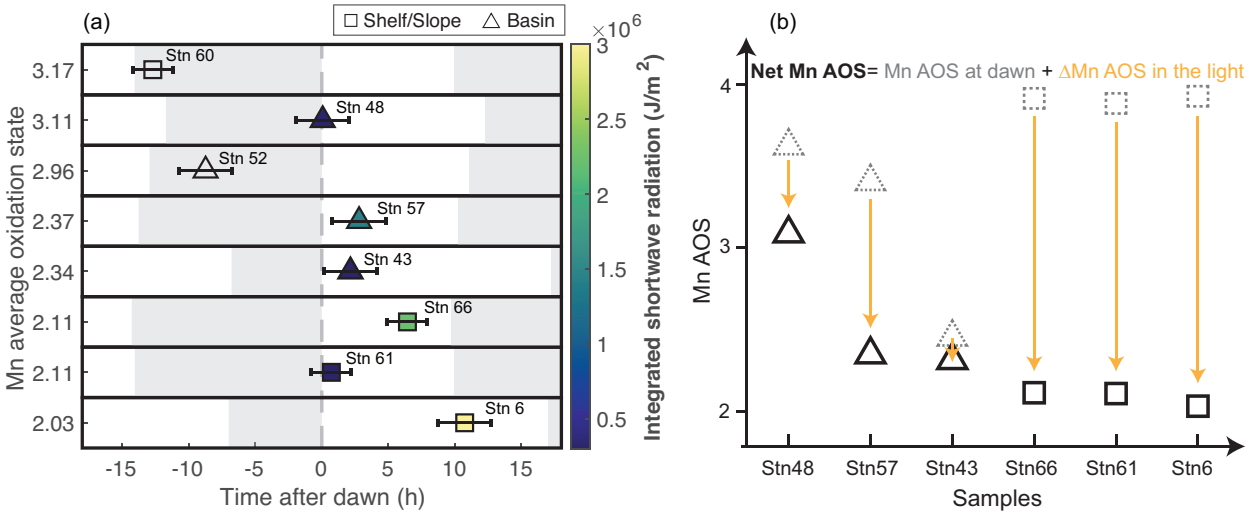

Figure 4. The relationship between time after dawn (unit: hour) and pMn AOS (a), and a schematic diagram of AOS during the day-night cycle (b). Shelf/slope and basin stations are marked as squares and triangles respectively. In panel (a), the length of night is indicated by the shaded rectangle for each station and the color bar is the integrated shortwave radiation (unit: J/m^2) from dawn to the end of particle sampling. Error bars demonstrate the period of in-situ particle sampling in the water column, typically 3-4 hours. The black solid symbols in (b) are the net pMn AOS measured by XANES, whereas grey dashed symbols are estimated AOS maxima at dawn (AOS_{dawn}) calculated based on the length of night and Mn oxidation rates.

Geophysical Research Letters

Supporting Information for

Diel Redox Cycle of Manganese in the Surface Arctic Ocean

Y. Xiang*, P. J. Lam, J. M. Lee

Department of Ocean Sciences, University of California, Santa Cruz, CA 95064 USA

Contents of this file

Additional Supporting Information (Files uploaded separately)

Introduction

The supporting information for this paper consists of three main elements: a detailed description of the method used to find three Mn reference minerals, seven supplemental figures, four supplemental tables (two uploaded separately). Supplemental tables contain information about the light conditions, particulate Mn concentrations, Mn XANES reference and sample spectra, and Mn average oxidation states derived from the synchrotron analysis.

Text S1.

Overall, there are 18 Mn mineral references in our library (Table S3), including spectra of Mn minerals that we collected at Beamline 11-2 (e.g., pyroxmangite ($Mn^{II}SiO_3$), hureaulite ($Mn^{II}_5(PO_3OH)_2(PO_4)_2 \cdot 4H_2O$)), those shared by collaborators (e.g., δ -$Mn^{IV}O_2$, feitknechtite ($Mn^{III}OOH$), Mn(II)-citrate), and the most reduced surface sample, GT11010s at Station 26, which was smoothed using a smoothing parameter of 2 using SIXPACK. Linear combination fitting (LCF) of sample XANES spectra (Table S4) in the energy range of 6520-6600 eV was conducted using different combinations of Mn mineral references using the Least Sq. Fitting module in SIXPACK (Webb, 2005). The goodness of the LSF fit was evaluated by the magnitude of the R-factor (Newville, 2001). The particulate Mn (pMn) average oxidation state (AOS) was calculated as a weighted average of Mn(II), Mn(III), and Mn(IV) using the LCF fractions of three end-member Mn references chosen to represent each oxidation state. The Mn references used as end members for AOS calculations were GT11010s-Mn(II), feitknechtite ($Mn^{III}OOH$), and δ-$Mn^{IV}O_2$. We chose these three Mn reference minerals for the following two reasons. First, compared to the most reduced surface sample GT11010s, none of the other Mn(II) references in our library, including a number of Mn silicates and Mn-organic ligand complexes, showed the characteristic absorption peak at 6551 eV as seen in surface pMn samples in the Arctic Ocean (Figure S6 & Table S2). Secondly, to choose appropriate oxidized Mn mineral references for our surface Arctic dataset, we applied LCF to the XANES spectrum of a pMn sample from the dark halocline (GT10800s; 176 m at Station 14) thought to be dominated by oxidized pMn (c.f., Xiang & Lam, 2020), also analyzed at Beamline 11-2. The LCF of this sample with two endmembers, feitknechtite ($Mn^{III}OOH$) and δ-$Mn^{IV}O_2$, led to a low R factor (Newville, 2001) of 7.56×10^{-4} (Figure S4), suggesting that these two references are reasonable choices to represent Mn(III) and Mn(IV) in the Western Arctic Ocean. Indeed,

feitknechtite ($Mn^{III}OOH$), and δ-$Mn^{IV}O_2$ are commonly used as Mn(III/IV) reference compounds in lab settings (Learman et al., 2011) and other ocean environments (Hermans et al., 2019; Lee et al., 2021; Oldham et al., 2021). We also would like to note that the primary purpose of calculating AOS is to define a metric to describe the variation in the speciation of pMn in the surface Arctic, rather than to give an accurate and precise estimate of pMn AOS. Given the lack of sample duplicates and beam time, the uncertainties in the values of pMn AOS calculated from the XANES spectra could not be formally assessed during this study. However, major variations in spectral features are clear and consistent with the trend of calculated pMn AOS (Figure 3).

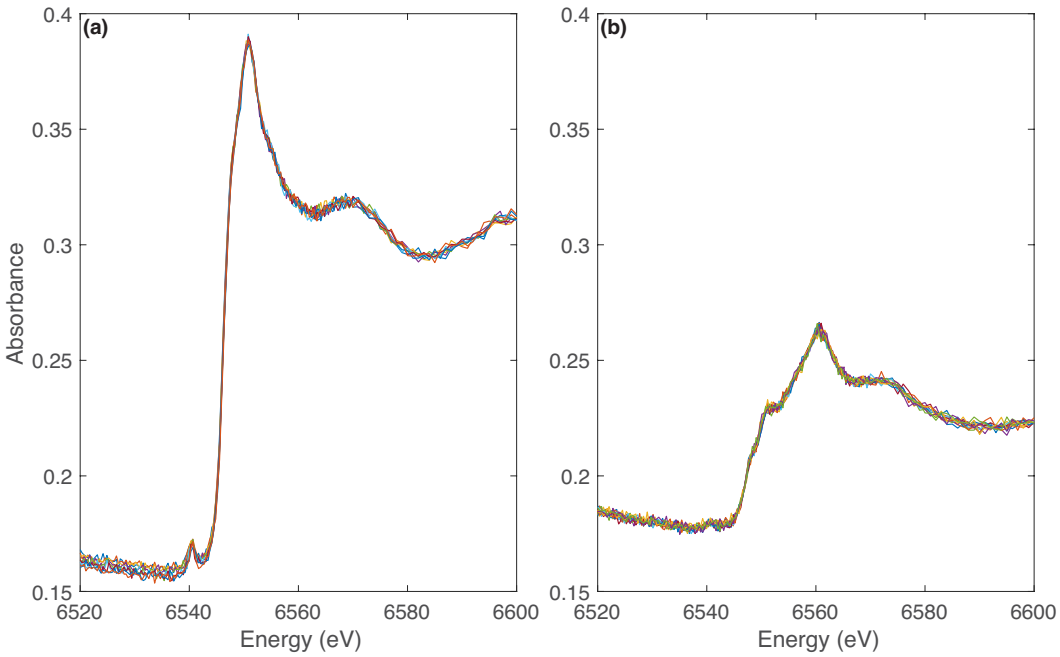

Figure S1. Raw Mn spectra of (a) one reduced pMn sample at Station 19 (9 scans over 1.5 hours) and (b) one oxidized sample at Station 48 (12 scans over 2 hours). No obvious energy shifts were observed in either sample over the course of the analyses, indicating no clear X-ray beam-induced photoreduction.

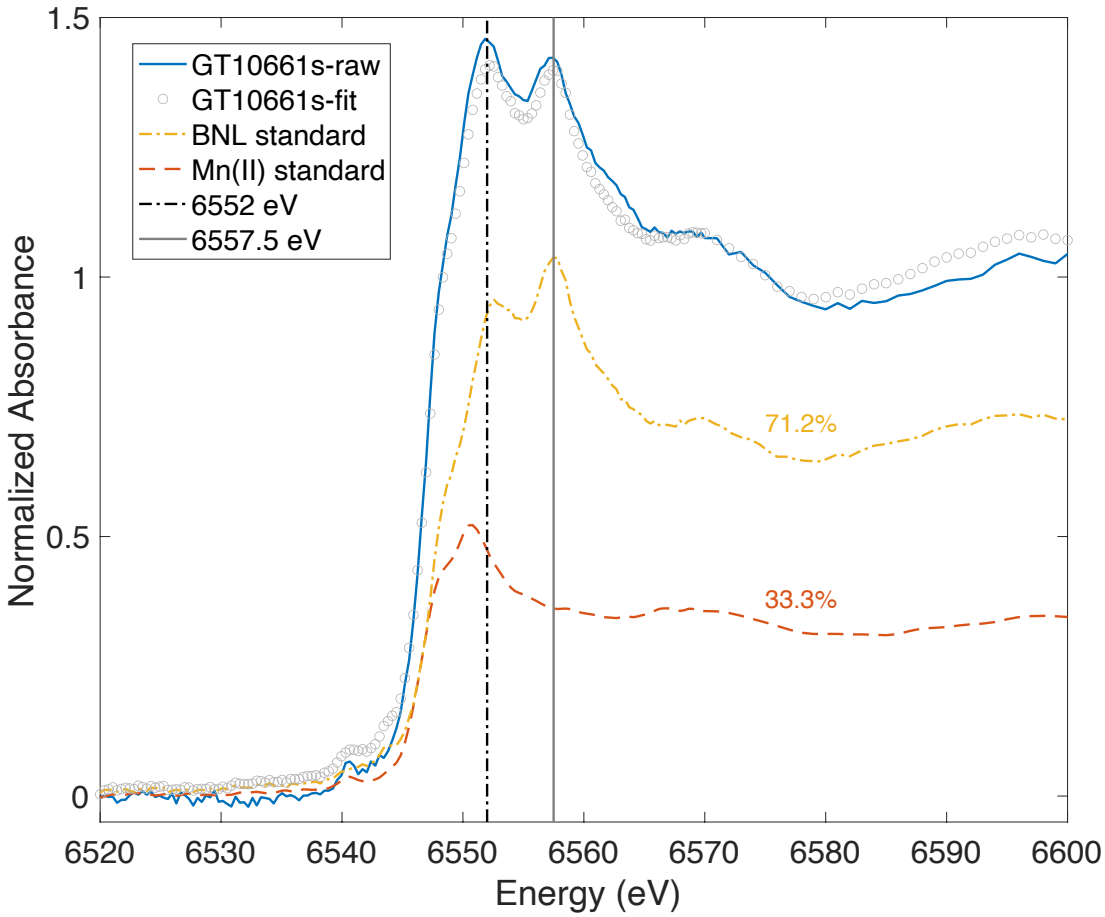

Figure S2. Linear combination fit (LCF) for surface sample GT10661s at Station 6 with the benthic nepheloid layer (BNL) sample (GT12276s), Mn(II) (GT11010s), Mn(III) (feitknechtite), and Mn(IV) (δ-MnO_2) references in the LCF. The fraction of the BNL reference (assumed to be Mn silicates) in the fit is 71.20% (68.11% if normalized to 1), and Mn(II) (GT11010s) is 33.34% (31.89% if normalized to 1). The fractions of feitknechtite and δ-MnO_2 are negligible. The R factor is 0.0014. Vertical black dash-dot and grey solid lines at 6552 eV and 6557.5 eV, respectively, for reference.

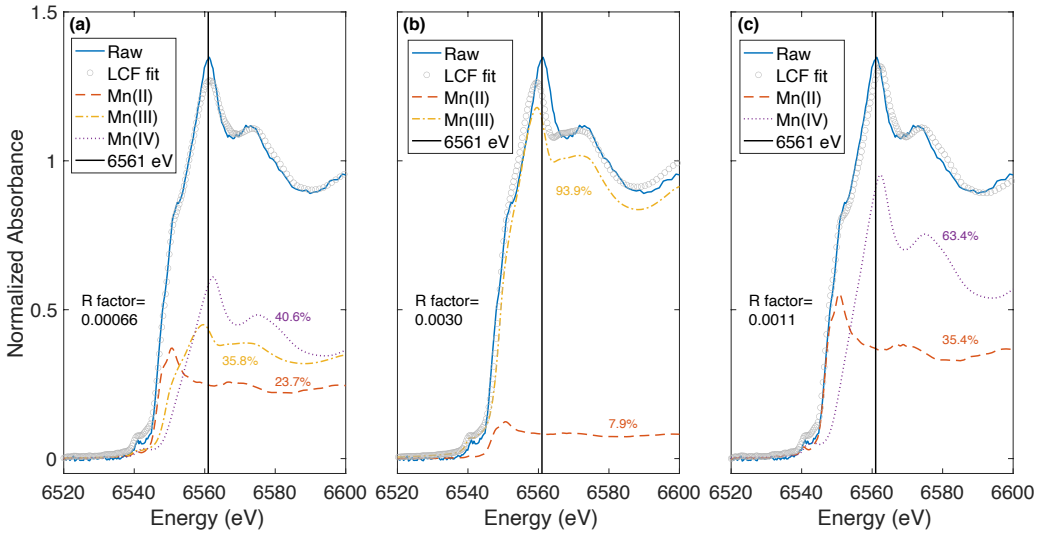

Figure S3. Linear combination fit for oxidized sample GT12240s at Station 60 with (a) Mn(II) (GT11010s), Mn(III) (feitknechtite), and Mn(IV) (δ-MnO_2) references, (b) GT11010s and feitknechtite only, and (c) GT11010s and δ-MnO_2 only in the fit. The fractions for different references (not normalized to 1) and R factor for the fit are displayed in each subplot. Better fits are characterized by smaller R factors. Vertical black solid lines at 6561 eV for reference.

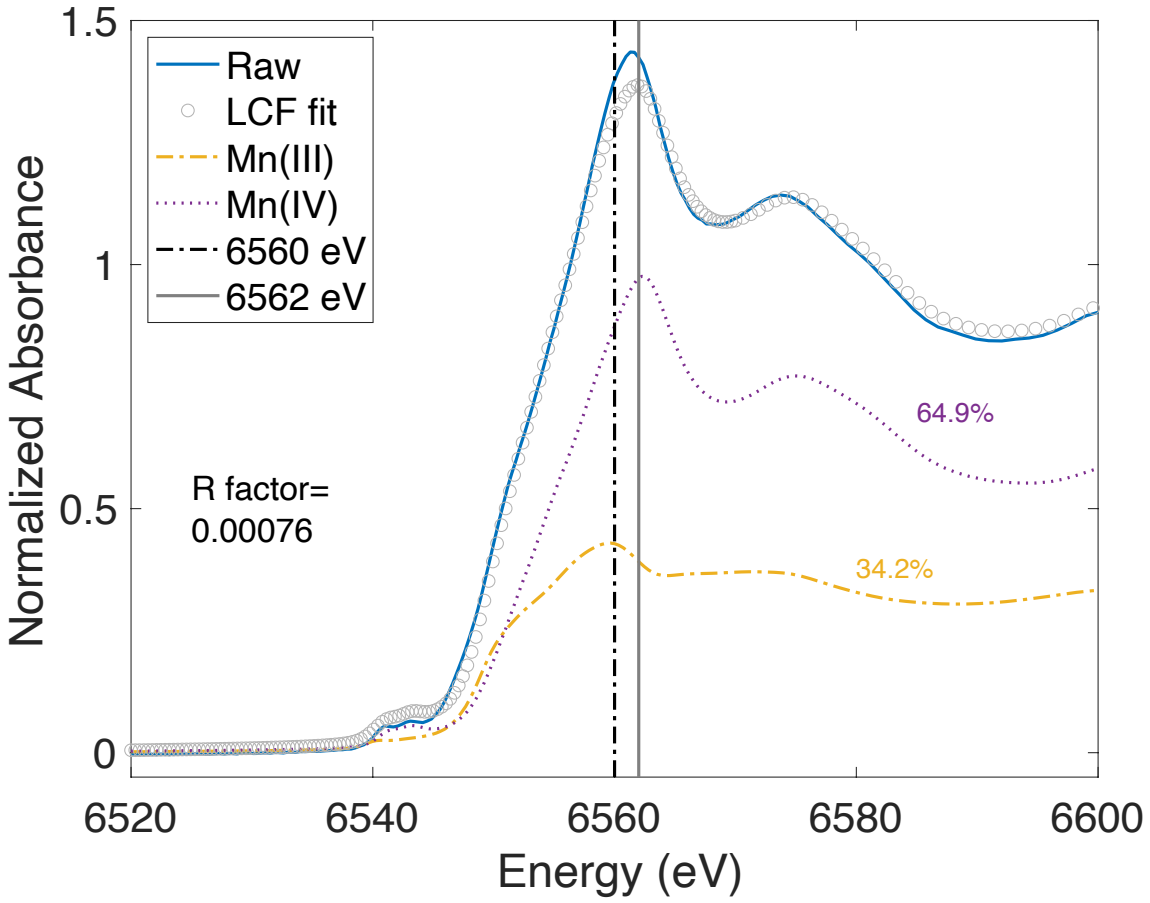

Figure S4. Linear combination fit for the most oxidized sample GT10800s in the halocline at Station 14 using Mn(III) (feitknechtite), and Mn(IV) (δ-MnO_2) as Mn references. The fit fractions for different references and R factor for the fit are displayed. Vertical black dash-dot and grey solid lines at 6560 eV and 6562 eV, respectively, for reference.

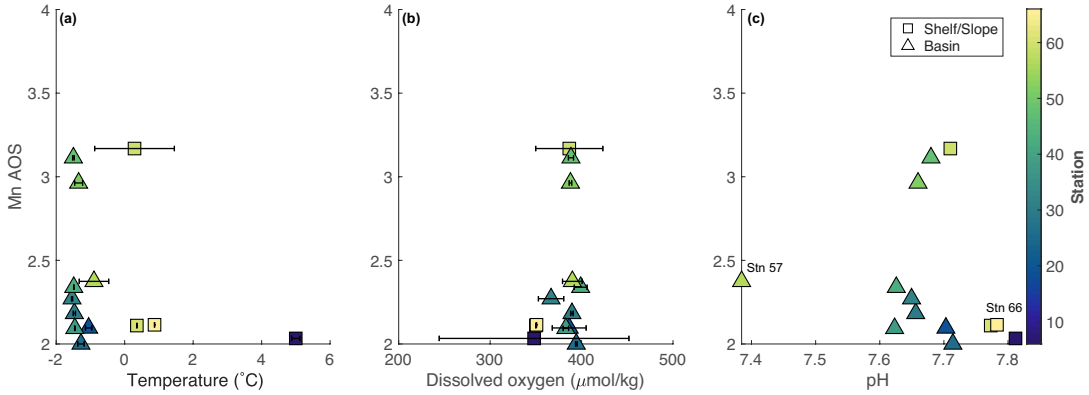

Figure S5. Scatter plots between Mn Average Oxidation State (AOS) from pumps and hydrographic parameters (a) Temperature (˚C); (b) dissolved oxygen (μmol/kg); (c) pH from the CTD rosette at pressure = 20 decibars. Mn AOS were determined on particles collected from pump

casts. Temperature and oxygen were collected from sensors mounted on the ODF CTD rosette and are plotted as the mean (marker) and standard deviation (error bars) of all CTD casts (N=1-7) from that station; pH was determined from discrete samples from one of the ODF CTD casts (Woosley et al., 2017) and linearly interpolated to 20 decibars. The multiple ODF CTD casts at each station generally spanned a similar range of light conditions as experienced by pump casts, so the mean and range should be a good indication of temperature and dissolved oxygen during particle sampling. Underway surface seawater measurements give additional evidence about the minor diel variation of temperature and dissolved oxygen in the Western Arctic Ocean, especially in the basin (data not shown). Measurements of pH were only made from one ODF CTD cast, but this was fortuitously frequently at similar light conditions as the pump cast, except for stations 57 and 66, when the pH data were from nighttime and the pump casts were during the day. The lowest pH observed at 20 decibars is from Station 57 (7.38), but it may not indicate strong remineralization in-situ at night, since the pH values measured at night in the surface of more productive slope Station 60 and shelf Station 66 are both higher than 7.65. Such low pH values can be reached within the strong benthic nepheloid layer (BNL) at shelf Station 61. Likely, the large pH difference between Station 57 and other basin station is due to lateral transport of a low pH water mass from the shelf BNL to Station 57.

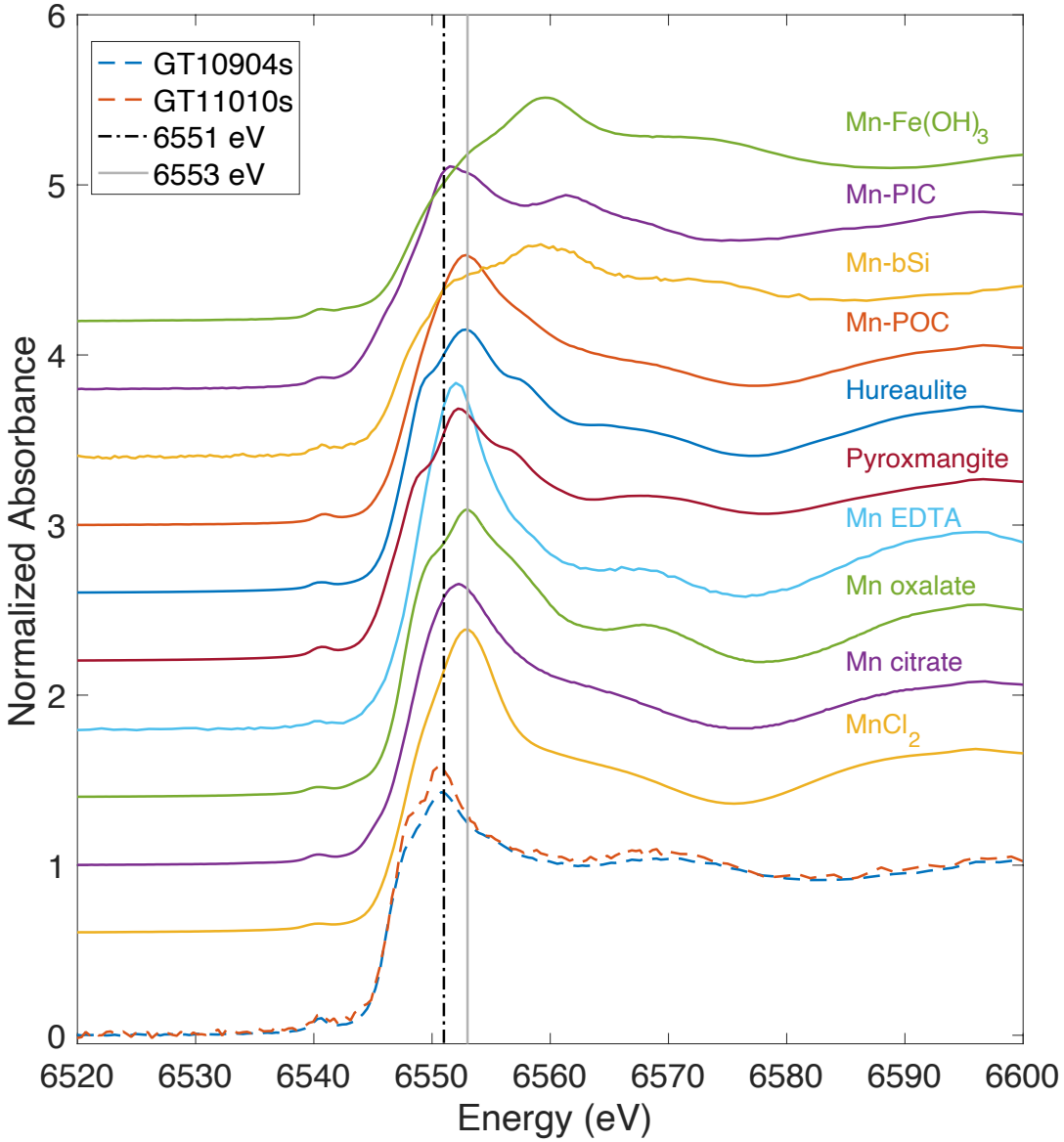

Figure S6. XANES spectra of the two most reduced surface samples, GT11010s at Station 26 and GT10904s at Station 19 (spectra with dashed lines) and six Mn(II) mineral references and four $MnCl_2$ adsorption standards (spectra with solid lines). Mn(II) references plotted include inorganic Mn ($MnCl_2$), organically bound Mn (Mn-citrate, -oxalate, and -EDTA), Mn silicates (Pyroxmangite), and Mn phosphates (Hureaulite). Mn-citrate and -oxalate spectra were obtained at the Australian Synchrotron (Blamey et al., 2018). We applied +1 eV energy shift observed in hausmannite ($Mn^{II}Mn^{III}_2O_4$) XANES spectrum to correct for the energy difference between SSRL and the Australian Synchrotron. Mn EDTA was measured at the Brazilian Synchrotron Light Laboratory (LNLS) (Machado et al., 2019). No obvious energy offset was observed between SSRL and LNLS based on Mn foil standards. Sorbed Mn standards we made and ran at Beamline 11-2 at SSRL include four major particle phases, particulate organic carbon (POC) from cultures of green algae,

clean diatom frustules, particulate inorganic carbon (PIC) from cleaned foraminifera shells, and synthesized 2-line ferrihydrite (Lee et al., 2021). Vertical black dash-dot and grey solid lines at 6551 eV and 6553 eV, respectively, for reference.

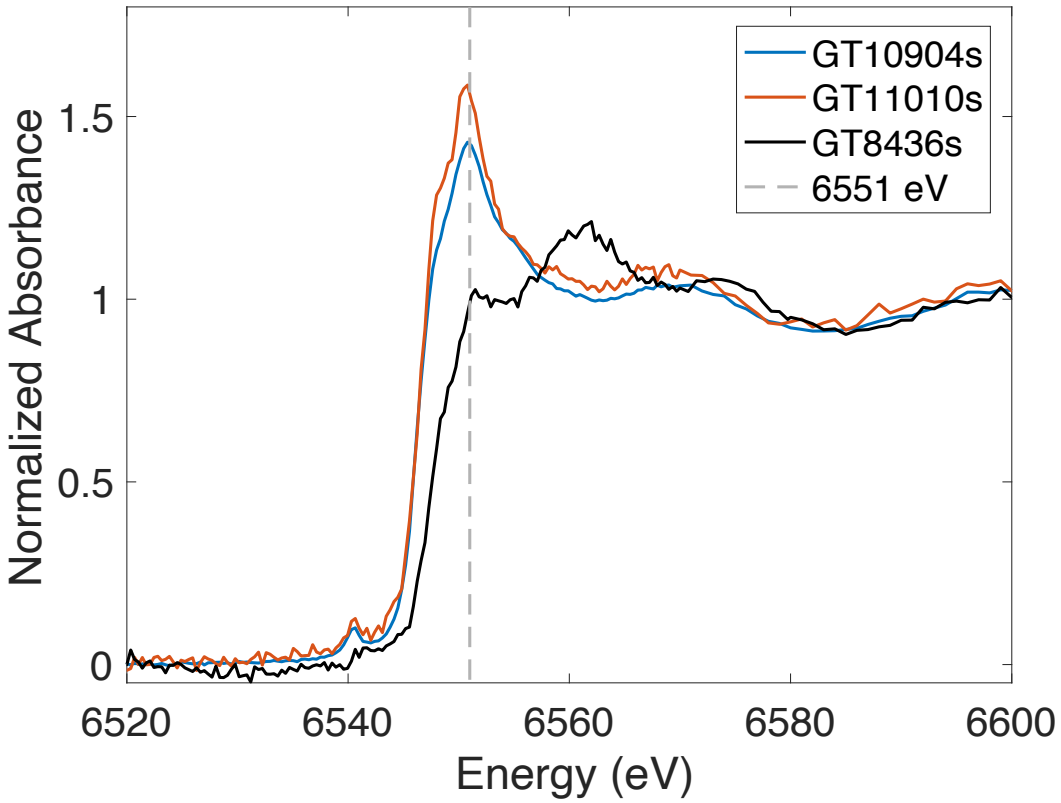

Figure S7. XANES spectra of the two most reduced surface samples, GT11010s at Station 26 and GT10904s at Station 19 in the GN01, and the unknown Mn mineral that contains pMn(II) in a neutrally buoyant hydrothermal plume from 15˚S East Pacific Rise collected from the U.S. GEOTRACES GP16 cruise (Lee et al., 2021).

Table S1. Sampling locations, light conditions, and particulate Mn concentration and average oxidation state of particles collected by in-situ pumps in the surface of the Western Arctic Ocean (uploaded separately).

Name	White line position	Sources
GT11010s (the most reduced surface sample)	6551 eV	This study
Mn adsorption standard (particulate inorganic carbon)	6552 eV	Lee et al. (2021)
Pyroxmangite	6552 eV	Lee et al. (2021)
Mn(II) citrate_PK	6552 eV	Blamey et al. (2018)
Mn(II) EDTA_HC	6552 eV	Machado et al. (2019)
Mn adsorption standard (particulate organic carbon)	6553 eV	Lee et al. (2021)
Hureaulite	6553 eV	Lee et al. (2021)
$MnCl_2$_CH	6553 eV	Learman et al. (2011)
Mn(II) oxalate_PK	6553 eV	Blamey et al. (2018)
Mn(II)-Siderophores	6553 eV	Harrington et al. (2012)
Mn-SOD	6554 eV	Gunter et al. (2006)
Mn adsorption standard (biogenic silica)	6559 eV	Lee et al. (2021)
Mn adsorption standard (ferrihydrite)	6560 eV	Lee et al. (2021)

Table S2. Summary of white line positions for Mn superoxide dismutase (SOD), adsorbed, inorganic and organically bound Mn XANES reference spectra. No references were found with a white line as low as observed for GT11010s.

Reference name	Formula
Mn(II) oxide	$Mn^{II}O$
Mn(II) sulfide	$Mn^{II}S$
Hureaulite	$Mn^{II}_5(PO_3OH)_2(PO_4)_2 \cdot 4H_2O$
Pyroxmangite	$Mn^{II}SiO_3$
Chalcophanite_CH	$ZnMn^{IV}_3O_7 \cdot 3H_2O$
δ-MnO_2_CH	δ-$Mn^{IV}O_2$
Feitknechtite_CH	$Mn^{III}O(OH)$
GT11010s-Mn(II)	Unknown Mn(II) phases
Hausmannite_CH	$Mn^{II}Mn^{III}_2O_4$
Manganese chloride_CH	$Mn^{II}Cl_2$
Mn foil_CH	Mn^0
Mn citrate_PK	Mn(II)-citrate
Mn oxalate_PK	Mn(II)-oxalate
Mn EDTA_HC	Mn(II)-EDTA
DBK1 spessartine_22_24_fl_JJ	$Mn^{II}_3Al_2(SiO_4)_3$
Hotazel_Braunite_009_fl_JJ	$Mn^{II}Mn^{III}_6(SiO_4)O_8$
PiemontiteGRR_039_fl_JJ	$\{Ca_2\}\{Al_2Mn^{III}\}(Si_2O_7)(SiO_4)O(OH)$
PiemontitieGRR_2_040_fl_JJ	$\{Ca_2\}\{Al_2Mn^{III}\}(Si_2O_7)(SiO_4)O(OH)$

Table S3. Mn mineral references in the current library (N=18). See Text S1 for further details.

Table S4. Mn XANES spectra sample and reference spectra used in the calculation of Mn average oxidation state (uploaded separately).